BIPOLAR DISORDERS
AN INTERNATIONAL JOURNAL OF PSYCHIATRY AND NEUROSCIENCES

Bipolar Disorders 2011: 13: 414–424

Brief Report

Tract-specific white matter structural disruption in patients with bipolar disorder

Benedetti F, Absinta M, Rocca MA, Radaelli D, Poletti S, Bernasconi A, Dallaspezia S, Pagani E, Falini A, Copetti M, Colombo C, Comi G, Smeraldi E, Filippi M. Tract-specific white matter structural disruption in patients with bipolar disorder.
Bipolar Disord 2011: 13: 414–424. © 2011 The Authors.
Journal compilation © 2011 John Wiley & Sons A/S.

Objectives: A growing body of evidence suggests that, independent of localized brain lesions, mood disorders can be associated with dysfunction of brain networks involved in the modulation of emotional and cognitive behavior. We used diffusion tensor (DT) tractography to quantify the presence and extent of structural injury to the connections between the amygdala and other brain regions, which included the subgenual, the supragenual and posterior cingulate, the parahippocampal, the orbitofrontal and dorsolateral prefrontal cortices, as well as the insula.

Methods: Using a 3.0 Tesla scanner, conventional and DT magnetic resonance imaging sequences of the brain were acquired from 15 adult patients with major depressive disorder (MDD), 15 with bipolar disorder (BD), and 21 age-matched healthy controls. Using FSL software, diffusivity changes of the white matter (WM) fiber bundles belonging to the emotional network were measured.

Results: Compared to controls and MDD patients, BD patients had significantly decreased average fractional anisotropy, increased average mean diffusivity, and increased average axial and radial diffusivity values in the majority of the WM fiber bundles connecting structures of the anterior limbic network (p-values ranging from 0.002 to 0.040). Medication load did not influence the results with the exception of lithium, which was associated with normal diffusivity values in tracts connecting the amygdala with the subgenual cingulate cortex.

Conclusions: We detected specific WM abnormalities, suggestive of disrupted integrity of fiber bundles in the brains of patients with BD. These abnormalities might contribute to understanding both mood dysregulation and cognitive disturbances in BD, and might provide an objective marker to monitor treatment efficacy in this condition.

Francesco Benedetti[a,b], Martina Absinta[b,c], Maria A Rocca[b,c], Daniele Radaelli[a,b], Sara Poletti[a,b,d], Alessandro Bernasconi[a,b], Sara Dallaspezia[a,b], Elisabetta Pagani[b,c], Andrea Falini[b,e], Massimiliano Copetti[f], Cristina Colombo[a], Giancarlo Comi[b,c], Enrico Smeraldi[a,b] and Massimo Filippi[b,c]

[a]Department of Clinical Neurosciences, Scientific Institute and University Vita-Salute San Raffaele,[b]C.E.R.M.A.C. (Centro di Eccellenza Risonanza Magnetica ad Alto Campo), University Vita-Salute San Raffaele,[c]Neuroimaging Research Unit, Institute of Experimental Neurology, Division of Neuroscience, Scientific Institute and University Vita-Salute San Raffaele, Milan,[d]Dipartimento di Scienze Farmacologiche, Università degli Studi di Palermo, Palermo,[e]Department of Neuroradiology, Scientific Institute and University Vita-Salute San Raffaele, Milan,[f]Biostatistics Unit, IRCCS-Ospedale Casa Sollievo della Sofferenza, San Giovanni Rotondo, Foggia, Italy

doi: 10.1111/j.1399-5618.2011.00938.x

Key words: amygdala – bipolar disorder – cingulate – diffusion tensor imaging – fractional anisotropy – major depression – tractography – white matter

Received 5 March 2010, revised and accepted for publication 3 June 2011

Corresponding author:
Dr. Francesco Benedetti
Istituto Scientifico Ospedale San Raffaele
Department of Clinical Neurosciences
San Raffaele Turro
Via Stamira d'Ancona 20
20125, Milano, Italy
Fax: +39-02-26433265
E-mail: benedetti.francesco@hsr.it

Structural and functional brain imaging studies allow for definition of a network of structures associated with emotional processing in healthy humans. The amygdala is a core component and several corticolimbic structures interact in the generation and regulation of affective states (1, 2). This network is sometimes referred to as the

The authors of this paper do not have any commercial associations that might pose a conflict of interest in connection with this manuscript.

anterior limbic network (3, 4) and mood disorders might possibly be associated with dysfunction of this network. It is also possible that emotional dysregulation could result from a lack of inhibition by prefrontal cortices (PFC) on limbic structures, as suggested by (i) the observation of decreased glucose metabolism in the PFC with increased metabolism in subcortical structures (5), and (ii) functional magnetic resonance imaging (MRI) studies showing reduced activity and impaired signal communication in corticolimbic networks critical to processing emotional stimuli (6, 7).

It has been speculated that disrupted functional connectivity could be associated with white matter (WM) pathology. Diffusion tensor (DT) MRI measures the extension and direction of water diffusivity, and provides indices of WM integrity which are sensitive to the subtle pathological changes associated with several neurological and psychiatric conditions (8). Two metrics of the diffusion properties that are commonly employed as indices of tissue pathology are mean diffusivity (MD), which measures the magnitude of water molecule diffusion, and fractional anisotropy (FA), which is an index of the degree of directionality of water diffusivity. FA is reduced in diseased states known to be associated with axonal loss and destruction of myelin sheaths (9). Axonal damage is reflected by a decrease of diffusivity parallel to the primary fiber orientation [axial diffusivity (AD)], while myelin breakdown is associated with an increased diffusivity perpendicular to the WM tract [radial diffusivity (RD)] with preserved AD values (10, 11).

DT MRI studies hold significant promise for the investigation of WM pathology associated with mood disorders (12). In patients with bipolar disorder (BD), decreased FA has been reported in WM tracts linking the PFC with other regions, without changes in trace apparent diffusion coefficient (13). This observation suggests a loss of bundle coherence and alignment of WM fibers without a significant amount of tissue disruption or reactive gliosis. Other studies observed increased water diffusivity (14), also with normal FA (15), in the PFC. In anterior regions, the majority of studies found reduced FA (16–25), however, some studies found an increased FA (26–28) and three studies reported lower or higher FA values depending on the brain regions which were assessed (26, 29, 30).

Few studies have been performed in patients with major depressive disorder (MDD). All of these report a widespread pattern of reduced FA values in late-life depression (31–38), but much less severe abnormalities in young and adult patients (39, 40).

DT MRI based tractography allows for reconstruction of anatomically complex WM pathways (41), but thus far, tract-specific studies in mood disorders are lacking. The only two reported studies were carried out in patients with BD and the researchers found an increased connectivity between the subgenual cingulate cortex and the amygdala (42), and reduced FA values in the uncinate fasciculi and anterior thalamic radiations (19). To explain these inconsistencies, one can hypothesize that the characteristics of WM damage might be influenced by the unipolar/bipolar dychotomy and might differ across the examined brain regions.

Therefore, to test the above hypotheses, we applied DT MRI tractography in order to compare the integrity of several individual WM tracts, known to be part of the anterior corticolimbic networks, between healthy subjects and patients with BD and MDD.

Methods

Participants

The study sample included 51 participants: 30 consecutively admitted inpatients affected by mood disorder that were screened with the Structured Clinical Interview for DSM Disorders (DSM-IV), and 21 age-matched healthy controls. Of the 30 inpatients, 15 of them met criteria for MDD (10 women and 5 men; mean age = 50.5 years, range: 37–63 years; disease duration = 19.7 years, range: 3–45 years; mean number of previous illness episodes = 3.0, range: 1.0–10.0) and 15 met criteria for BD type I (10 women and 5 men; mean age = 48.4 years, range: 23–64 years; disease duration = 12.4 years, range: 0.2–31.0 years; mean number of previous illness episodes = 4.4, range: 2.0–11.0). Exclusion criteria were: (i) additional diagnoses on Axis I, (ii) mental retardation on Axis II, (iii) current pregnancy, or (iv) major medical or neurological disorders. Physical examinations, laboratory tests, and electrocardiograms were performed on each study participant. No patient had received electroconvulsive therapy (ECT) within six months prior to study enrollment though four patients had received it during their lifetime. All patients had been admitted to our hospital ward during a major depressive episode and were studied prior to discharge. Their current symptom profile was of remission (Hamilton Rating Scale for Depression scores < 8) after receiving successful antidepressant treatment. At the time of the study, patients were being treated based on their clinical need: for BD [lithium (n = 8; patients on

lithium had been taking it for at least six months), valproate (n = 2), carbamazepine (n = 1), antidepressants (n = 11), antipsychotics (n = 6)], and for MDD [antidepressants (n = 15)]. All patients were also receiving benzodiazepines. To assess the potential effect of the psychotropic medication load on WM fiber bundle integrity, we used previously developed criteria and categorized each medication into low-dose or high-dose groupings, scored as 0 (no medication), 1 (low dosage), or 2 (high dosage). We then combined all individual medication scores for each medication category in each individual participant to obtain a single composite score (30).

A total of 21 age-matched healthy subjects (10 women and 11 men; mean age = 46.4 years, range: 27–67 years) with no previous history of psychiatric, neurological, and/or systemic disorders served as controls. After complete description of the study to all subjects, written informed consent was obtained and the study was approved by the local Ethical Committee.

Image acquisition

Using a 3.0 Tesla scanner (Intera, Philips Medical Systems, Best, The Netherlands), the following sequences of the brain were obtained from all subjects: (i) T2-weighted turbo spin echo (TSE) [TR/TE = 3000/85 msec; echo train length = 15; flip angle = 90°; 25 contiguous, 5 mm-thick, axial slices with a matrix size = 512 × 512, and a field of view (FOV) = 230 x 183.28 mm]; (ii) 3D T1-weighted fast field echo (FFE) [TR/TE = 25/4.6 msec; flip angle = 30°; 220 contiguous, axial slices with voxel size = 0.89 × 0.89 × 0.8 mm (matrix size = 256 × 256; FOV = 230 × 230 mm); (iii) sensitivity-encoded (SENSE) pulsed-gradient SE echo planar (EP) (acceleration factor = 2.0; TR/TE = 8753.89/58 msec; 55 contiguous, 2.3-mm thick axial slices with an acquisition matrix size = 128 × 128, and a FOV = 240 × 240 mm^2; after SENSE reconstruction, the matrix dimension of each slice was 128 × 128, and in-plane pixel size 1.87 × 1.87 mm^2), with diffusion gradients applied in 35 noncollinear directions and a b-factor = 900 sec/mm^2. Fat saturation was performed to avoid chemical shift artifacts. All slices were positioned to run parallel to a line that joins the most infero-anterior and infero-posterior parts of the corpus callosum.

Structural MRI post-processing

All structural MRI analysis was performed by a single experienced observer, unaware to whom the scans belonged. Aspecific brain hyperintensities were identified on the T2-weighted TSE scans and their volumes were measured using a semiautomatic local thresholding segmentation technique (Jim 4.0, Xinapse System, Leicester, UK).

Head motion effect and image distortion due to eddy current were corrected. After reconstruction of brain DT MRI data, MD and FA maps were derived for every pixel. Probabilistic modeling of diffusion parameters and tractography were carried out using the methods from the FMRIB Diffusion Toolkit (FDT) implemented in the Functional Magnetic Resonance Imaging of the Brain Software Library (http://www.fmrib.ox.ac.uk/fsl) (43, 44). In detail, the first step was the Bayesian Estimation of Diffusion Parameters Obtained using Sampling Techniques [bedpostx (the *x* stands for modeling crossing fibres)] that run Markov Chain Monte Carlo sampling to build up distributions on diffusion parameters at each voxel and created all the files necessary for running probabilistic tractography. After bedpostx had been applied, it was possible to run tractography analyses using probtrackx tool (5,000 streamline samples, 0.5 mm step lengths, curvature thresholds = 0.2).

Tractography analysis

In order to initiate and constrain tractography, eight brain regions were selected based on an *a priori* knowledge of their interactions in the emotional network (45–47). For each subject and in each hemisphere, the amygdala, orbitofrontal cortex (BA11), subgenual cingulate cortex (BA25), parahippocampal cortex (BA36), posterior cingulate cortex (BA23), supragenual cingulate cortex (BA32), lateral prefrontal cortex (BA46), and insula were identified. Amygdala was segmented automatically from the 3D T1-weighted scans, using the FMRIB's Integrated Registration and Segmentation Tool (FIRST). The results of the segmentation were inspected visually to check for correctness. The other brain regions were segmented using the VTK CISG Registration Toolkit (48) and an affine transformation. The Broadman regions were taken from Broadman template provided by SPM5 (49, 50), whereas the insula was obtained from the aal template also provided by SPM5 (51). These atlases were first coregistered to the 3D T1-weighted scans of each subject, and then to the diffusion space using a rigid transformation (Fig. 1).

In each hemisphere, the following WM fiber bundles, as defined by their initial and target regions were reconstructed: amygdala-BA11,

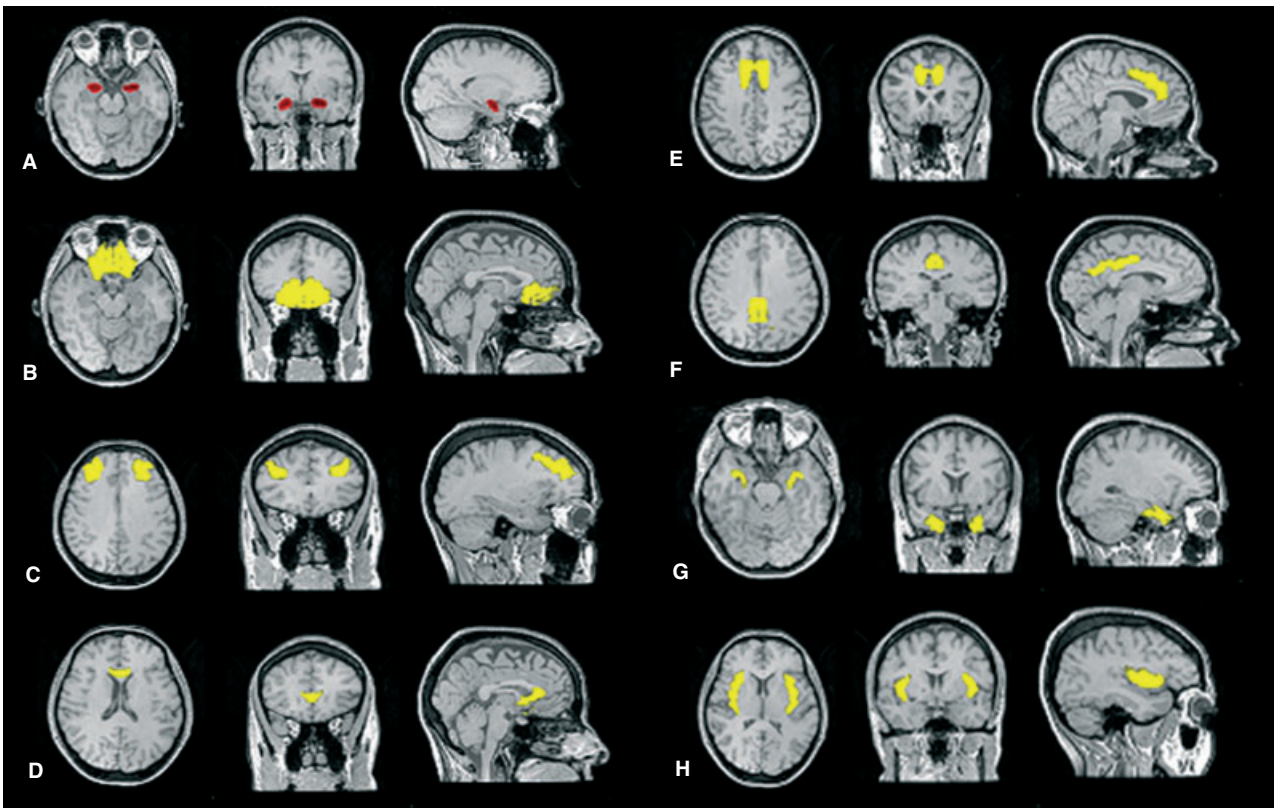

Fig. 1. An illustrative example of cortical masks in a subject of the: (A) amygdala, (B) orbitofrontal cortex (BA11), (C) lateral prefrontal cortex (BA46), (D) subgenual cingulate (BA25), (E) supragenual cingulate (BA32), (F) posterior cingulate (BA23), (G) parahippocampal cortex (BA36), and (H) insula. The amygdala (red) was segmented automatically from the 3D T1-weighted scans, using the FMRIB's Integrated Registration and Segmentation Tool. The other brain regions (yellow) were segmented using the VTK CISG Registration Toolkit (48) and an affine transformation.

amygdala-BA25, amygdala-BA36, amygdala-insula, BA23-BA32, BA25-BA32, BA11-BA46, and BA25-insula (Fig. 2). To have an *internal* patient reference, the corticospinal tracts (CST) were also reconstructed, using the cerebral peduncle as seed mask, which was segmented manually from the FA maps, and using BA4 as the target cortical mask.

An exclusion mask was produced in order to limit the propagation of the tractography in the WM and to avoid indirect connections between gray matter (GM) nuclei as well as those of crossing fibers to the controlateral hemisphere. Such a mask was obtained by adding the masks of CST, thalami, and mid-sagittal plane. In each subject, CST was segmented with the FMRIB's Automated Segmentation Tool from T2-weighted, but not from diffusion weighted images. The thalami were segmented with FIRST on the 3D T1-weighted scans.

The output of the tractography algorithm was a probabilistic map which provides, at each voxel, a connectivity value corresponding to the total number of samples that pass from the seed to the target region through that given voxel. For each connectivity map the mean value of connectivity was assessed (52). In addition, the reconstructed WM fiber bundles were also applied as masks to the MD, FA, AD (which is equivalent to the magnitude of the largest eigenvalue of the tensor), and RD (which is the average of the two smallest eigenvalues of the tensor), and average values were calculated.

Statistical analysis

Patients' WM fiber bundle derived measures were reported as mean ± standard deviation. Differences according to the disease status were assessed with analysis of variance (ANOVA) models. Adjustments for multiple comparisons were accounted for using the Bonferroni method considering each of the eight tracts as a family. Furthermore, the post-hoc comparisons between patients versus healthy controls were carried out within the ANOVA models and Bonferroni was adjusted as above.

To assess the effect of demographic and clinical characteristics on diffusivity parameters, the tract-specific measures, that were found to be significantly different between groups after adjustment for multiple comparisons, were correlated with age,

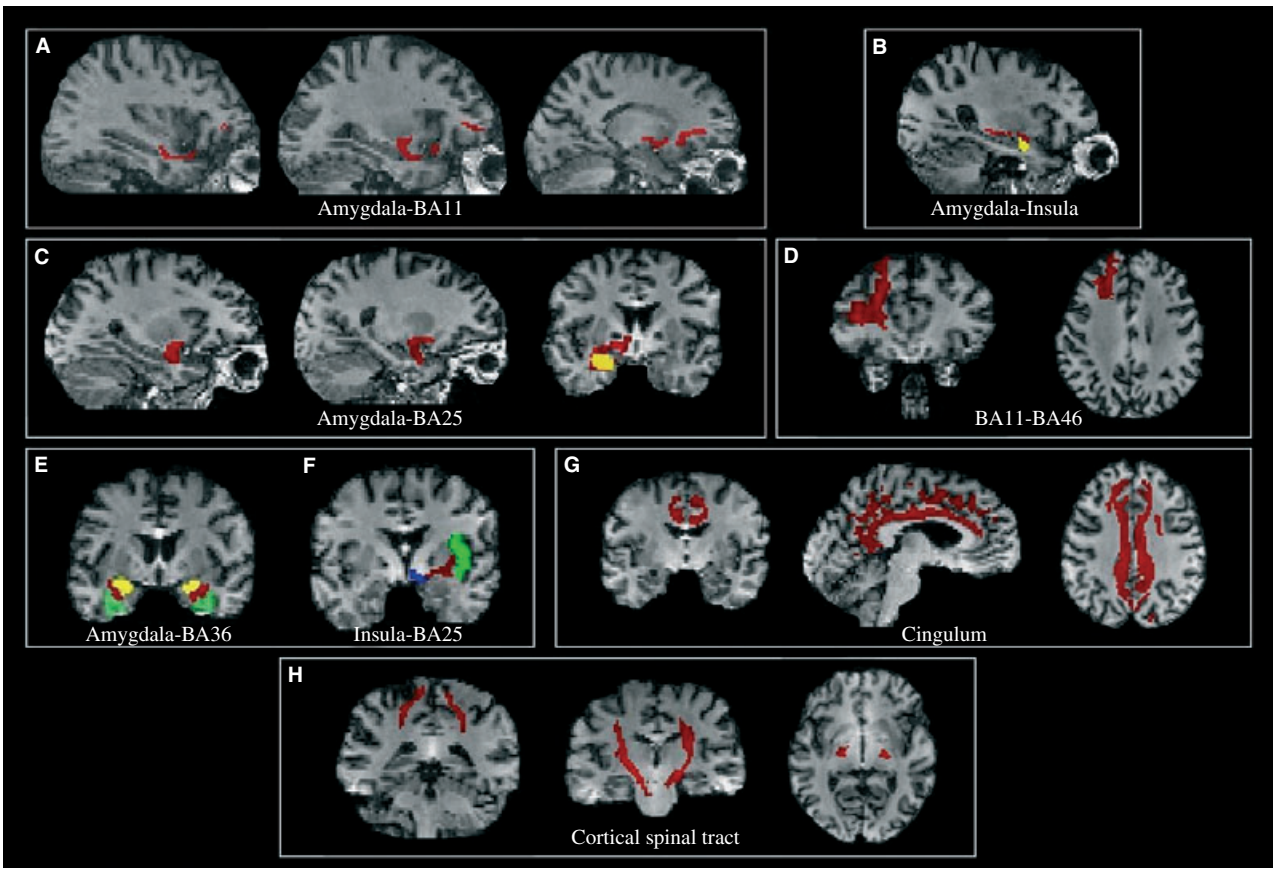

Fig. 2. An illustrative example of tract reconstruction (red) in a single subject of the: (A) amygdala-orbitofrontal cortex (BA11), (B) amygdala-insula, (C) amygdala-subgenual cingulate cortex [(BA25); amygdala in yellow], (D) orbitofrontal cortex (BA11)–lateral prefrontal cortex (BA46), (E) amygdala–BA36 (amygdala in yellow, BA36 in green), (F) insula-subgenual cingulate cortex [(BA25); insula in green, BA25 in blue], (G) cingulum, and (H) corticospinal tracts.

age at onset, medication load, and lifetime rate of illness recurrence (number of previous illness episodes/duration of illness in years). Correlations between continuous variables were assessed using Spearman coefficients.

A p-value < 0.05 was considered for statistical significance. All analyses were performed using SAS Release 9.1 (SAS Institute, Cary, NC, USA).

Results

No significant difference was found between MDD and BD patients in terms of age, sex, disease duration, and mean relapse number. Brain aspecific hyperintensities were seen on the T2-weighted MRI scans of 8 healthy controls, 9 MDD patients, and 11 BD patients. The median T2 brain hyperintense lesion load was 0.0 ml (range: 0.0–5.8 ml) in healthy controls, 0.7 ml (range: 0.0–2.5 ml) in MDD patients, and 0.6 ml (range: 0.0–1.0 ml) in BD patients (p = n.s.).

Tract-specific DT MRI derived quantities are summarized in Table 1 and Figure 3. Significant between-group differences were found for FA and AD of the amygdala-BA25 connection, bilaterally; for MD, AD, and RD of the BA32-BA23 connection; for MD of the left BA11-BA46 connection; for MD and AD of the right BA25-insula connection; and for RD of the BA25-BA32 connection. The connectivity values of all the analyzed WM fiber bundles did not differ between groups (data not shown). When contrasted to healthy subjects at post-hoc analysis, BD patients had significantly lower average FA and significantly higher average MD, average AD and RD values of all the WM fiber bundles reported above (p-values ranging from 0.002 to 0.040). No significant differences were found between MDD patients and healthy controls.

The overall medication load score was not correlated with any of the tract-specific measures that were found to be significantly different from those of healthy controls (data not shown). Also, the scores of specific drug classes were not correlated with diffusivity parameters, with the exception of lithium. Patients treated with lithium showed significantly higher FA values in the amygdala-BA25 connection than those who did not receive lithium (0.32 ± 0.02 versus

Table 1. Diffusion tensor magnetic resonance imaging measures [mean (SD)] in healthy controls (HC) and patients with bipolar disorder (BD) and major depressive disorder (MDD), and levels of significance of the observed differences, uncorrected for multiple comparisons

	HC	BD	MDD	p-value ANOVA
R Amyg-BA25 FA[a,b,c]	0.35 (0.06)	0.30 (0.03)	0.32 (0.05)	0.003
L Amyg-BA25 FA[c,d]	0.37 (0.08)	0.31 (0.02)	0.34 (0.04)	0.01
R Amyg-BA25 MD	0.88 (0.06)	0.88 (0.04)	0.87 (0.04)	0.9
L Amyg-BA25 MD	0.90 (0.08)	0.89 (0.04)	0.86 (0.05)	0.08
R Amyg-BA25 AD	1.23 (0.09)	1.17 (0.06)	1.18 (0.05)	0.3
L Amyg-BA25 AD	1.19 (0.18)	1.18 (0.06)	1.18 (0.05)	0.08
R Amyg-BA25 RD	0.70 (0.07)	0.74 (0.04)	0.72 (0.05)	0.2
L Amyg-BA25 RD	0.71 (0.07)	0.74 (0.03)	0.70 (0.06)	0.2
R Amyg-BA25 voxels, n	709 (576)	693 (284)	706 (347)	0.9
L Amyg-BA25 voxels, n	520 (381)	553 (244)	568 (270)	0.9
R Amyg-BA11 FA	0.32 (0.06)	0.30 (0.02)	0.31 (0.03)	0.7
L Amyg-BA11 FA	0.29 (0.07)	0.30 (0.03)	0.31 (0.05)	0.7
R Amyg-BA11 MD	0.85 (0.05)	0.87 (0.05)	0.86 (0.05)	0.4
L Amyg-BA11 MD	0.89 (0.08)	0.88 (0.08)	0.87 (0.07)	0.8
R Amyg-BA11 AD	1.14 (0.04)	1.16 (0.06)	1.15 (0.04)	0.6
L Amyg-BA11 AD	1.17 (0.08)	1.17 (0.10)	1.16 (0.08)	0.9
R Amyg-BA11 RD	0.70 (0.07)	0.73 (0.04)	0.72 (0.05)	0.4
L Amyg-BA11 RD	0.75 (0.10)	0.69 (0.20)	0.72 (0.07)	0.5
R Amyg-BA11 voxels, n	629 (305)	588 (382)	573 (361)	0.6
L Amyg-BA11 voxels, n	459 (233)	492 (395)	381 (258)	0.06
R Amyg-Insula FA	0.39 (0.07)	0.38 (0.05)	0.38 (0.07)	0.9
L Amyg-Insula FA	0.37 (0.05)	0.34 (0.05)	0.37 (0.06)	0.1
R Amyg-Insula MD	0.82 (0.10)	0.85 (0.05)	0.83 (0.06)	0.2
L Amyg-Insula MD	0.82 (0.07)	0.86 (0.04)	0.84 (0.04)	0.1
R Amyg-Insula AD	1.17 (0.06)	1.22 (0.07)	1.19 (0.06)	0.07
L Amyg-Insula AD	1.17 (0.07)	1.18 (0.06)	1.18 (0.07)	0.7
R Amyg-Insula RD	0.64 (0.08)	0.67 (0.07)	0.65 (0.09)	0.5
L Amyg-Insula RD	0.65 (0.08)	0.70 (0.05)	0.61 (0.20)	0.1
R Amyg-Insula voxels, n	975 (691)	1658 (1283)	1328 (1294)	0.08
L Amyg-Insula voxels, n	1017 (943)	1661 (1590)	705 (722)	0.2
R Amyg-BA36 FA	0.33 (0.04)	0.35 (0.05)	0.32 (0.03)	0.1
L Amyg-BA36 FA	0.34 (0.05)	0.31 (0.06)	0.33 (0.02)	0.3
R Amyg-BA36 MD	0.86 (0.05)	0.80 (0.20)	0.85 (0.04)	0.4
L Amyg-BA36 MD	0.86 (0.05)	0.80 (0.20)	0.86 (0.04)	0.4
R Amyg-BA36 AD	1.17 (0.07)	1.21 (0.06)	1.16 (0.06)	0.09
L Amyg-BA36 AD	1.17 (0.05)	1.17 (0.07)	1.17 (0.07)	0.9
R Amyg-BA36 RD	0.70 (0.06)	0.69 (0.05)	0.70 (0.04)	0.8
L Amyg-BA36 RD	0.70 (0.06)	0.72 (0.05)	0.70 (0.04)	0.5
R Amyg-BA36 voxels, n	1683 (1062)	2000 (1569)	2785 (1458)	0.06
L Amyg-BA36 voxels, n	1867 (1437)	2210 (1554)	1889 (1110)	0.8
R BA11-BA46 FA	0.35 (0.04)	0.34 (0.03)	0.35 (0.04)	0.8
L BA11-BA46 FA	0.34 (0.03)	0.34 (0.03)	0.36 (0.03)	0.3
R BA11-BA46 MD	0.78 (0.03)	0.79 (0.03)	0.79 (0.03)	0.3
L BA11-BA46 MD[c,e]	0.79 (0.03)	0.81 (0.03)	0.79 (0.02)	0.03
R BA11-BA46 AD	1.08 (0.05)	1.09 (0.04)	1.09 (0.03)	0.06
L BA11-BA46 AD	1.09 (0.04)	1.12 (0.05)	1.11 (0.02)	0.8
R BA11-BA46 RD	0.63 (0.03)	0.64 (0.03)	0.64 (0.04)	0.3
L BA11-BA46 RD	0.63 (0.04)	0.66 (0.03)	0.63 (0.03)	0.09
R BA11-BA46 voxels, n	2279 (1592)	2376 (1183)	2299 (1295)	0.5
L BA11-BA46 voxels, n	2903 (1588)	3200 (1490)	2628 (1118)	0.9
R BA25-Insula FA	0.36 (0.03)	0.36 (0.02)	0.36 (0.03)	0.8
L BA25-Insula FA	0.36 (0.03)	0.35 (0.03)	0.37 (0.02)	0.09
R BA25-Insula MD[c,f]	0.82 (0.05)	0.87 (0.07)	0.84 (0.05)	0.04
L BA25-Insula MD	0.81 (0.05)	0.85 (0.04)	0.83 (0.03)	0.09
R BA25-Insula AD[c,e]	1.15 (0.08)	1.22 (0.10)	1.18 (0.03)	0.03
L BA25-Insula AD	1.14 (0.07)	1.17 (0.04)	1.18 (0.03)	0.1
R BA25-Insula RD	0.65 (0.05)	0.69 (0.06)	0.66 (0.04)	0.09
L BA25-Insula RD	0.65 (0.05)	0.68 (0.04)	0.66 (0.03)	0.1
R BA25-Insula voxels, n	4009 (1482)	4617 (2181)	4667 (1641)	0.4
L BA25-Insula voxels, n	3958 (1751)	4715 (1536)	4784 (1955)	0.3

Table 1. (Continued)

	HC	BD	MDD	p-value ANOVA
BA25-BA32 FA	0.37 (0.03)	0.35 (0.03)	0.38 (0.03)	0.08
BA25-BA32 MD	0.79 (0.03)	0.83 (0.10)	0.78 (0.03)	0.06
BA25-BA32 AD	1.12 (0.04)	1.16 (0.10)	1.14 (0.02)	0.2
BA25-BA32 RD[c,g]	0.62 (0.04)	0.67 (0.08)	0.62 (0.04)	0.02
BA25-BA32 voxels, n	4944 (1910)	5408 (2523)	4970 (1298)	0.7
BA32-BA23 FA	0.33 (0.03)	0.32 (0.03)	0.33 (0.02)	0.5
BA32-BA23 MD[a,h,i]	0.75 (0.02)	0.78 (0.02)	0.76 (0.03)	0.002
BA32-BA23 AD[c,f]	1.03 (0.05)	1.07 (0.04)	1.05 (0.04)	0.04
BA32-BA23 RD[a,j,k]	0.61 (0.02)	0.64 (0.03)	0.62 (0.03)	0.009
BA32-BA23 voxels, n	4969 (1487)	5570 (1298)	5864 (1171)	0.1
R CST FA	0.48 (0.05)	0.50 (0.05)	0.52 (0.05)	0.1
L CST FA	0.48 (0.05)	0.48 (0.05)	0.51 (0.03)	0.3
R CST MD	0.73 (0.03)	0.74 (0.02)	0.73 (0.02)	0.6
L CST MD	0.74 (0.04)	0.76 (0.03)	0.76 (0.03)	0.1
R CST AD	1.17 (0.07)	1.20 (0.05)	1.20 (0.05)	0.2
L CST AD	1.18 (0.06)	1.21 (0.07)	1.23 (0.04)	0.06
R CST RD	0.52 (0.04)	0.51 (0.04)	0.51 (0.04)	0.2
L CST RD	0.53 (0.04)	0.54 (0.05)	0.53 (0.03)	0.6
R CST voxels, n	802 (337)	713 (430)	773 (369)	0.06
L CST voxels, n	815 (333)	735 (282)	787 (412)	0.06

Average mean diffusivity (MD), axial diffusivity (AD), and radial diffusivity (RD) values are expressed in units of $mm^2/sec \times 10^{-3}$. Fractional anisotropy (FA) is a dimensionless index. R = right; L = left; Amyg = amygdala; BA25 = subgenual cingulate; BA11 = orbitofrontal cortex; BA36 = parahippocampal cortex; BA46 = lateral prefrontal cortex; BA32 = supragenual cingulate; BA23 = posterior cingulate; CST = corticospinal tract.
[a]Significant also after correction for multiple comparisons.
[b]p = 0.0008 (BD versus HC).
[c]BD versus MDD: not significant.
[d]p = 0.004 (BD versus HC).
[e]p = 0.008 (BD versus HC).
[f]p = 0.01 (BD versus HC).
[g]p = 0.009 (BD versus HC).
[h]p = 0.0006 (BD versus HC).
[i]p = 0.02 (BD versus MDD).
[j]p = 0.003 (BD versus HC).
[k]p = 0.03 (BD versus MDD).

0.28 ± 0.02, $p = 0.01$). The comparison between BD patients with and without ongoing lithium versus healthy controls showed that the same measures behaved differently in the two diseased groups ($F = 6.55$, $p = 0.004$), with lithium-treated patients having values not significantly different than those of healthy controls, and lithium-free patients having significantly lower values than those of healthy controls (post-hoc Newman-Keuls test, $p = 0.009$).

The rate of lifetime illness recurrence correlated directly with increased MD of the right BA25-insula connection ($r = 0.48$, $p = 0.02$). Age was significantly and directly correlated with MD ($r = 0.47$, $p = 0.009$) of the BA32-BA23 connection.

Discussion

This is the first tractography study assessing DT MRI parameters in multiple brain WM tracts of patients affected by mood disorders. We found that patients with BD have alterations which are likely to reflect disruption of myelin sheaths (i.e., increase of mean and RD) in WM tracts connecting subgenual, supragenual, and posterior areas of cingulate cortex. Moreover, patients showed decreased FA values (which are likely to reflect decreased bundle coherence as well as disrupted myelin) in tracts connecting amygdala and subgenual cingulate cortex, bilaterally.

Previous findings based on a variety of functional neuroimaging techniques (functional MRI, positron emission tomography, single photon emission computerized tomography) showed that an abnormal functioning of these brain structures might be involved in the psychopathology of mood disorders (4, 7, 45, 53, 54). Our findings in BD patients provide a possible structural basis to these observations. Damage of critical WM tracts connecting cortical areas might hamper connectivity

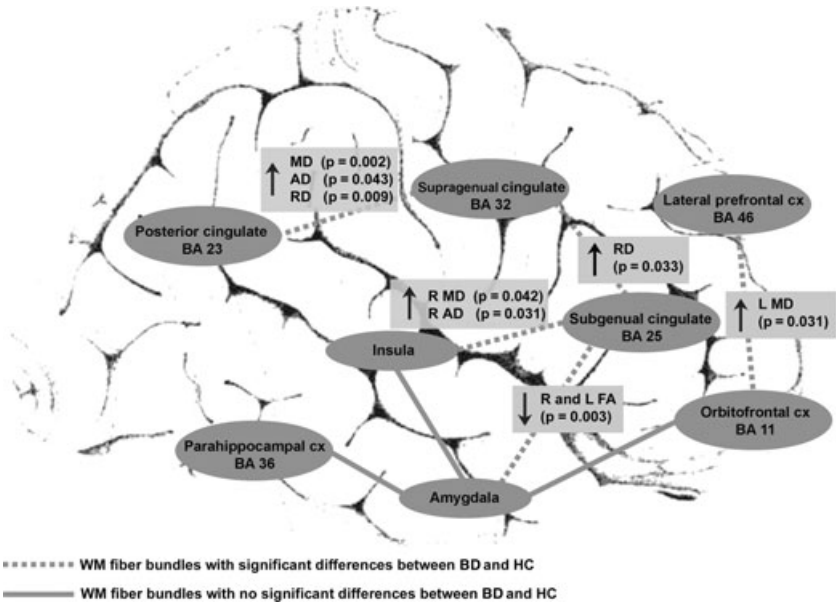

Fig. 3. Graphical representation of white matter (WM) fiber bundles analyzed and of the observed differences between patients with bipolar disorder (BD) and healthy controls (HC). Only structural measures significantly different between groups have been reported. MD = mean diffusivity; AD = axial diffusivity; RD = radial diffusivity; FA = fractional anisotropy; R = right; L = left.

between them and disregulate brain networks involved in mood and emotions (Fig. 3). The WM tracts in which we found abnormal DT MRI measures include (i) uncinate fasciculus, which directly connects the hippocampus, amygdala, and temporal poles to the subgenual cortex (55), and where we observed bilaterally reduced FA in the fibers linking amygdala and BA 25; (ii) cingulum, along which we observed increased RD both in anterior and posterior regions; and (iii) prefrontal cortico-cortical WM fibers connecting orbitofrontal and lateral prefrontal cortex. Our tract-specific observations are in agreement with previous reports of abnormal DT MRI measures in the uncinate fasciculus, cingulum, and short prefrontal fibers in patients with BD (13, 16–25). Our findings support the hypothesis of an impaired connection between the amygdala and the cingulate and prefrontal cortical areas, which play a major role in resolving emotional conflict (56), and in inhibiting amygdala responses to negative emotional stimuli (46).

The nature of the injury leading to these abnormalities remains elusive. A similar pattern of abnormal DT MRI parameters has been detected in conditions associated with inflammation, degeneration, demyelination, and dysmyelination (57).

An altered myelination during development, resulting in abnormal MRI findings early in the pediatric stage, has been proposed to play a role in the pathophysiology of BD (58). In addition, postmortem gene expression, neuropathological, and neuroimaging studies suggest down-regulation of key oligodendrocyte and myelination genes (59), as well as lowered density of oligodendroglial cells in BD patients (60). Finally, several findings suggest an altered immune function affecting myelin maintenance and repair (12), which is likely to be important in the pathophysiology of the disease (61).

Interestingly, we observed a protective effect of ongoing lithium treatment in terms of relatively preserved FA values in the WM tracts connecting amygdala with subgenual cingulate cortex. Considering that we observed that the rate of recurrence of illness episodes had an opposite detrimental effect, this observation suggests that lithium is likely to counteract the neuropathological process associated with WM changes in BD. In patients with BD, lithium has been reported to increase GM density in the cingulate cortex and paralimbic structures (62), thus normalizing the abnormally reduced GM volumes associated with the disease (63). Lithium affects myelin gene expression (64), and a previous DT MRI study assessing the effect of lithium on WM integrity showed that this drug is associated with diffusely increased FA and decreased MD values in the brain of patients with human immunodeficiency virus infection (65). In this study, we suggest that the protective effect of lithium could extend to the WM changes associated with BD (see 12, 66).

We did not observe either significant differences, or abnormal trends, between MDD patients and healthy controls. Although the relatively small

sample size studied and the high clinical heterogeneity of this condition (67) do not allow us to draw definite conclusions, this observation is in agreement with previous reports of severe WM abnormalities in late-life MDD (see *Introduction*), and with those describing cognitive impairment in young patients with BD (68), but not in those with MDD (69).

In conclusion, we speculate that *critical* WM pathology is likely to be at least one of the pathological substrates of BD; that the observed WM changes might be secondary to disruption of the integrity of myelin sheaths; and that effective treatments for BD, such as lithium, may protect against such an injury. All of this suggests that WM diffusivity changes may be of clinical relevance in BD and that, in future studies, DT MRI might provide reliable markers of treatment efficacy in this psychiatric disorder.

Clearly, this study is not without limitations, including the relatively small number of recruited subjects, and the fact that we selected one of the available strategies for the analysis of our DT MRI data. Further research in larger independent samples is now warranted to clarify all of the issues raised by our findings.

Acknowledgements

The C.E.R.M.A.C. received research grants from The Italian Ministry of University and Scientific Research, the Italian Ministry of Health, Trenta ore per la Vita Association, the European Union (FP7 grant 222963), and Janssen-Cilag.

References

1. Phillips ML, Drevets WC, Rauch SL, Lane R. Neurobiology of emotion perception II: Implications for major psychiatric disorders. Biol Psychiatry 2003; 54: 515–528.
2. Phillips ML, Drevets WC, Rauch SL, Lane R. Neurobiology of emotion perception I: The neural basis of normal emotion perception. Biol Psychiatry 2003; 54: 504–514.
3. Strakowski SM, Delbello MP, Adler CM. The functional neuroanatomy of bipolar disorder: a review of neuroimaging findings. Mol Psychiatry 2005; 10: 105–116.
4. Adler CM, DelBello MP, Strakowski SM. Brain network dysfunction in bipolar disorder. CNS Spectr 2006; 11: 312–320.
5. Ketter TA, Kimbrell TA, George MS et al. Effects of mood and subtype on cerebral glucose metabolism in treatment-resistant bipolar disorder. Biol Psychiatry 2001; 49: 97–109.
6. Rich BA, Fromm SJ, Berghorst LH et al. Neural connectivity in children with bipolar disorder: impairment in the face emotion processing circuit. J Child Psychol Psychiatry 2008; 49: 88–96.
7. Benedetti F, Bernasconi A, Blasi V et al. Neural and genetic correlates of antidepressant response to sleep deprivation: a functional magnetic resonance imaging study of moral valence decision in bipolar depression. Arch Gen Psychiatry 2007; 64: 179–187.
8. Le Bihan D. Looking into the functional architecture of the brain with diffusion MRI. Nat Rev Neurosci 2003; 4: 469–480.
9. Kochunov P, Thompson PM, Lancaster JL et al. Relationship between white matter fractional anisotropy and other indices of cerebral health in normal aging: tract-based spatial statistics study of aging. Neuroimage 2007; 35: 478–487.
10. Pierpaoli C, Barnett A, Pajevic S et al. Water diffusion changes in Wallerian degeneration and their dependence on white matter architecture. Neuroimage 2001; 13: 1174–1185.
11. Song SK, Kim JH, Lin SJ, Brendza RP, Holtzman DM. Diffusion tensor imaging detects age-dependent white matter changes in a transgenic mouse model with amyloid deposition. Neurobiol Dis 2004; 15: 640–647.
12. Brambilla P, Bellani M, Yeh PH, Soares JC. Myelination in bipolar patients and the effects of mood stabilizers on brain anatomy. Curr Pharm Des 2009; 15: 2632–2636.
13. Adler CM, Holland SK, Schmithorst V et al. Abnormal frontal white matter tracts in bipolar disorder: a diffusion tensor imaging study. Bipolar Disord 2004; 6: 197–203.
14. Regenold WT, D'Agostino CA, Ramesh N, Hasnain M, Roys S, Gullapalli RP. Diffusion-weighted magnetic resonance imaging of white matter in bipolar disorder: a pilot study. Bipolar Disord 2006; 8: 188–195.
15. Beyer JL, Taylor WD, MacFall JR et al. Cortical white matter microstructural abnormalities in bipolar disorder. Neuropsychopharmacology 2005; 30: 2225–2229.
16. Wang F, Kalmar JH, Edmiston E et al. Abnormal corpus callosum integrity in bipolar disorder: a diffusion tensor imaging study. Biol Psychiatry 2008; 64: 730–733.
17. Wang F, Jackowski M, Kalmar JH et al. Abnormal anterior cingulum integrity in bipolar disorder determined through diffusion tensor imaging. Br J Psychiatry 2008; 193: 126–129.
18. Sussmann JE, Lymer GK, McKirdy J et al. White matter abnormalities in bipolar disorder and schizophrenia detected using diffusion tensor magnetic resonance imaging. Bipolar Disord 2009; 11: 11–18.
19. McIntosh AM, Muñoz Maniega S, Lymer GK et al. White matter tractography in bipolar disorder and schizophrenia. Biol Psychiatry 2008; 64: 1088–1092.
20. Frazier JA, Breeze JL, Papadimitriou G et al. White matter abnormalities in children with and at risk for bipolar disorder. Bipolar Disord 2007; 9: 799–809.
21. Pavuluri MN, Yang S, Kamineni K et al. Diffusion tensor imaging study of white matter fiber tracts in pediatric bipolar disorder and attention-deficit/hyperactivity disorder. Biol Psychiatry 2009; 65: 586–593.
22. Adler CM, Adams J, DelBello MP et al. Evidence of white matter pathology in bipolar disorder adolescents experiencing their first episode of mania: a diffusion tensor imaging study. Am J Psychiatry 2006; 163: 322–324.
23. Kafantaris V, Kingsley P, Ardekani B et al. Lower orbital frontal white matter integrity in adolescents with bipolar I disorder. J Am Acad Child Adolesc Psychiatry 2009; 48: 79–86.
24. Bruno S, Cercignani M, Ron MA. White matter abnormalities in bipolar disorder: a voxel-based diffusion tensor imaging study. Bipolar Disord 2008; 10: 460–468.
25. Chaddock CA, Barker GJ, Marshall N et al. White matter microstructural impairments and genetic liability to familial bipolar I disorder. Br J Psychiatry 2009; 194: 527–534.

26. Mahon K, Wu J, Malhotra AK et al. A voxel-based diffusion tensor imaging study of white matter in bipolar disorder. Neuropsychopharmacology 2009; 34: 1590–1600.
27. Yurgelun-Todd DA, Silveri MM, Gruber SA, Rohan ML, Pimentel PJ. White matter abnormalities observed in bipolar disorder: a diffusion tensor imaging study. Bipolar Disord 2007; 9: 504–512.
28. Wessa M, Houenou J, Leboyer M et al. Microstructural white matter changes in euthymic bipolar patients: a whole-brain diffusion tensor imaging study. Bipolar Disord 2009; 11: 504–514.
29. Haznedar MM, Roversi F, Pallanti S et al. Fronto-thalamo-striatal gray and white matter volumes and anisotropy of their connections in bipolar spectrum illnesses. Biol Psychiatry 2005; 57: 733–742.
30. Versace A, Almeida JR, Hassel S et al. Elevated left and reduced right orbitomedial prefrontal fractional anisotropy in adults with bipolar disorder revealed by tract-based spatial statistics. Arch Gen Psychiatry 2008; 65: 1041–1052.
31. Yang Q, Huang X, Hong N, Yu X. White matter microstructural abnormalities in late-life depression. Int Psychogeriatr 2007; 19: 757–766.
32. Taylor WD, MacFall JR, Payne ME et al. Late-life depression and microstructural abnormalities in dorsolateral prefrontal cortex white matter. Am J Psychiatry 2004; 161: 1293–1296.
33. Nobuhara K, Okugawa G, Sugimoto T et al. Frontal white matter anisotropy and symptom severity of late-life depression: a magnetic resonance diffusion tensor imaging study. J Neurol Neurosurg Psychiatry 2006; 77: 120–122.
34. Alexopoulos GS, Kiosses DN, Choi SJ, Murphy CF, Lim KO. Frontal white matter microstructure and treatment response of late-life depression: a preliminary study. Am J Psychiatry 2002; 159: 1929–1932.
35. Shimony JS, Sheline YI, D'Angelo G et al. Diffuse microstructural abnormalities of normal-appearing white matter in late life depression: a diffusion tensor imaging study. Biol Psychiatry 2009; 66: 245–252.
36. Bae JN, MacFall JR, Krishnan KR, Payne ME, Steffens DC, Taylor WD. Dorsolateral prefrontal cortex and anterior cingulate cortex white matter alterations in late-life depression. Biol Psychiatry 2006; 60: 1356–1363.
37. Murphy CF, Gunning-Dixon FM, Hoptman MJ et al. White-matter integrity predicts stroop performance in patients with geriatric depression. Biol Psychiatry 2007; 61: 1007–1010.
38. Yuan Y, Zhang Z, Bai F et al. White matter integrity of the whole brain is disrupted in first-episode remitted geriatric depression. Neuroreport 2007; 18: 1845–1849.
39. Ma N, Li L, Shu N et al. White matter abnormalities in first-episode, treatment-naive young adults with major depressive disorder. Am J Psychiatry 2007; 164: 823–826.
40. Kieseppä T, Eerola M, Mäntylä R et al. Major depressive disorder and white matter abnormalities: a diffusion tensor imaging study with tract-based spatial statistics. J Affect Disord 2010; 120: 240–244.
41. Rovaris M, Agosta F, Pagani E, Filippi M. Diffusion tensor MR imaging. Neuroimaging Clin N Am 2009; 19: 37–43.
42. Houenou J, Wessa M, Douaud G et al. Increased white matter connectivity in euthymic bipolar patients: diffusion tensor tractography between the subgenual cingulate and the amygdalo-hippocampal complex. Mol Psychiatry 2007; 12: 1001–1010.
43. Behrens TE, Johansen-Berg H, Woolrich MW et al. Non-invasive mapping of connections between human thalamus and cortex using diffusion imaging. Nat Neurosci 2003; 6: 750–757.
44. Behrens TE, Woolrich MW, Jenkinson M et al. Characterization and propagation of uncertainty in diffusion-weighted MR imaging. Magn Reson Med 2003; 50: 1077–1088.
45. Mayberg HS, Liotti M, Brannan SK et al. Reciprocal limbic-cortical function and negative mood: converging PET findings in depression and normal sadness. Am J Psychiatry 1999; 156: 675–682.
46. Pezawas L, Meyer-Lindenberg A, Drabant EM et al. 5-HTTLPR polymorphism impacts human cingulate-amygdala interactions: a genetic susceptibility mechanism for depression. Nat Neurosci 2005; 8: 828–834.
47. Stein JL, Wiedholz LM, Bassett DS et al. A validated network of effective amygdala connectivity. Neuroimage 2007; 36: 736–745.
48. Hartkens T, Rueckert D, Schnabel JA, Hawkes DJ, Hill DLG. VTK CISG Registration Toolkit: an open source software package for affine and non-rigid registration of single- and multimodal 3D images. In: Meiler M, Saupe D, Kruggel F eds. Bildverarbeitung für die Medizin 2002, Algorithmen-Systeme-Anwendungen. Leipzig: Springer-Verlag, 2002: 366–369.
49. Maldjian JA, Laurienti PJ, Kraft RA, Burdette JH. An automated method for neuroanatomic and cytoarchitectonic atlas-based interrogation of fMRI data sets. Neuroimage 2003; 19: 1233–1239.
50. Lancaster JL, Woldorff MG, Parsons LM et al. Automated Talairach atlas labels for functional brain mapping. Hum Brain Mapp 2000; 10: 120–131.
51. Tzourio-Mazoyer N, Landeau B, Papathanassiou D et al. Automated anatomical labeling of activations in SPM using a macroscopic anatomical parcellation of the MNI MRI single-subject brain. Neuroimage 2002; 15: 273–289.
52. Ciccarelli O, Behrens TE, Altmann DR et al. Probabilistic diffusion tractography: a potential tool to assess the rate of disease progression in amyotrophic lateral sclerosis. Brain 2006; 129: 1859–1871.
53. Hamann S. Blue genes: wiring the brain for depression. Nat Neurosci 2005; 8: 701–703.
54. Phillips ML, Ladouceur CD, Drevets WC. A neural model of voluntary and automatic emotion regulation: implications for understanding the pathophysiology and neurodevelopment of bipolar disorder. Mol Psychiatry 2008; 13: 829.
55. Schmahmann JD, Pandya DN, Wang R et al. Association fibre pathways of the brain: parallel observations from diffusion spectrum imaging and autoradiography. Brain 2007; 130: 630–653.
56. Etkin A, Egner T, Peraza DM, Kandel ER, Hirsch J. Resolving emotional conflict: a role for the rostral anterior cingulate cortex in modulating activity in the amygdala. Neuron 2006; 51: 871–882.
57. Alexander AL, Lee JE, Lazar M, Field AS. Diffusion tensor imaging of the brain. Neurotherapeutics 2007; 4: 316–329.
58. Caetano SC, Silveira CM, Kaur S et al. Abnormal corpus callosum myelination in pediatric bipolar patients. J Affect Disord 2008; 108: 297–301.
59. Tkachev D, Mimmack ML, Ryan MM et al. Oligodendrocyte dysfunction in schizophrenia and bipolar disorder. Lancet 2003; 362: 798–805.
60. Uranova NA, Vostrikov VM, Orlovskaya DD, Rachmanova VI. Oligodendroglial density in the prefrontal cortex in schizophrenia and mood disorders: a study from the

Stanley Neuropathology Consortium. Schizophr Res 2004; 67: 269–275.
61. Goldstein BI, Kemp DE, Soczynska JK, McIntyre RS. Inflammation and the phenomenology, pathophysiology, comorbidity, and treatment of bipolar disorder: a systematic review of the literature. J Clin Psychiatry 2009; 70: 1078–1090.
62. Bearden CE, Thompson PM, Dalwani M et al. Greater cortical gray matter density in lithium-treated patients with bipolar disorder. Biol Psychiatry 2007; 62: 7–16.
63. Sassi RB, Brambilla P, Hatch JP et al. Reduced left anterior cingulate volumes in untreated bipolar patients. Biol Psychiatry 2004; 56: 467–475.
64. McQuillin A, Rizig M, Gurling HM. A microarray gene expression study of the molecular pharmacology of lithium carbonate on mouse brain mRNA to understand the neurobiology of mood stabilization and treatment of bipolar affective disorder. Pharmacogenet Genomics 2007; 17: 605–617.
65. Schifitto G, Zhong J, Gill D et al. Lithium therapy for human immunodeficiency virus type 1-associated neurocognitive impairment. J Neurovirol 2009; 15: 176–186.
66. Beaulieu JM, Caron MG. Looking at lithium: molecular moods and complex behaviour. Mol Interv 2008; 8: 230–241.
67. Merikangas KR, Wicki W, Angst J. Heterogeneity of depression. Classification of depressive subtypes by longitudinal course. Br J Psychiatry 1994; 164: 342–348.
68. Pavuluri MN, West A, Hill SK, Jindal K, Sweeney JA. Neurocognitive function in pediatric bipolar disorder: 3-year follow-up shows cognitive development lagging behind healthy youths. J Am Acad Child Adolesc Psychiatry 2009; 48: 299–307.
69. Grant MM, Thase ME, Sweeney JA. Cognitive disturbance in outpatient depressed younger adults: evidence of modest impairment. Biol Psychiatry 2001; 50: 35–43.